Biomaterials 282 (2022) 121401

Contents lists available at ScienceDirect

Biomaterials

journal homepage: www.elsevier.com/locate/biomaterials

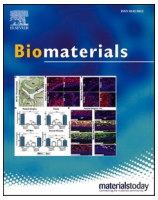

Nano-oxygenated hydrogels for locally and permeably hypoxia relieving to heal chronic wounds

Zhengyang Yang [a,1], Huanhuan Chen [c,1], Peizheng Yang [b,1], Xiaofei Shen [d,1], Yiqiao Hu [b], Yuhao Cheng [b,e,***], Hongwei Yao [a,**], Zhongtao Zhang [a,*]

[a] Department of General Surgery, Beijing Friendship Hospital, Capital Medical University, Beijing Key Laboratory of Cancer Invasion and Metastasis Research & National Clinical Research Center for Digestive Diseases, Beijing, 100050, China
[b] State Key Laboratory of Pharmaceutical Biotechnology, Medical School and School of Life Sciences, Nanjing University, Nanjing, 210093, China
[c] Key Laboratory of Biomedical Polymers of Ministry of Education & Department of Chemistry, Wuhan University, Wuhan, 430071, China
[d] Department of General Surgery, Drum Tower Hospital, Medical School of Nanjing University, Nanjing, 210008, China
[e] Jun Skincare Co. Ltd., Jiangsu Life Science & Technology Innovation Park, Nanjing, 210093, China

ARTICLE INFO

Keywords:
Chronic wound
Hypoxia
Oxygen delivery
Perfluorocarbon nanoparticle
Wound dressing

ABSTRACT

Exposed chronic wounds are usually covered by hypoxic tissues accompanied with necrosis, persistent inflammation and anaerobic infections. Since atmospheric oxygen air can only penetrate about 0.3 mm tissues, meanwhile oxygen from the circulation is difficult to reach chronic wounds through the destroyed blood vessels, a solution to deliver oxygen locally and permeably is urgently needed. Herein we report a technique to reform traditional gel-based wound dressings by adding lyophilized oxygen encapsulated nanoparticles, which can deliver dissolved oxygen locally into wound surface. This delivery technique can potentially evaluate the therapeutic effects on hypoxic epithelial, endothelial and fibroblasts *in vitro*. Further experiments confirm the effects on both open wounds bearing and flap transplanted diabetic mice models. Considering its biocompatibility, effectiveness and practicality, we believe our hydrogel has significant transformation value to care and accelerate the healing of various clinical wounds, especially chronic wound.

1. Introduction

As a widespread disease, diabetes has affected more than 400 million people worldwide, and the number of patients is expected to be more than 640 million by 2040 [1,2]. Diabetes complications, particularly chronic nonhealing wounds, have destructive effects on the quality of life and markedly increase social health care costs [3–5]. About 70% amputation limb amputations in worldwide are caused by diabetic foot ulcer, while continuously effective therapies are still absent in recent years [6–8]. Refractory nonhealing wounds in diabetes are primarily due to lower oxygenation, microvascular occlusion, bacterial colonization in a high glucose environment and peripheral neuropathy [9–11]. Among them, local wound hypoxia is a significant reason for poor wound healing [12,13].

Oxygen is indispensable in human energy production and can generate adenosine triphosphate through aerobic glycolysis [14,15]. During wound healing, sufficient oxygenation is critical because reparative processes such as collagen synthesis and attacking bacterial and cell multiplication require abundant energy [16,17]. However, the oxygen supply of diabetic chronic wounds is severely inadequate because of damaged blood vessels, permeation and high metabolic demands. In the necrotic area, tissue oxygen is usually less than 10 mmHg (while transcutaneous oxygen levels of normal tissue are approximately 40 mmHg) [18,19]. Existing methods, whether hyperbaric oxygen therapy or topical oxygen therapy, have difficulty relieving wound hypoxia [20,21]. Damaged blood vessels limit blood oxygen diffusion through circulation, and tissue tightness limits gaseous oxygen permeation into wounds. In these cases, the scheme of topical dissolved oxygen therapy

* Corresponding author.
** Corresponding author.
*** Corresponding author. State Key Laboratory of Pharmaceutical Biotechnology, Medical School and School of Life Sciences, Nanjing University, Nanjing, 210093, China.
E-mail addresses: chengyuhao@jun-skincare.com (Y. Cheng), yaohongwei@ccmu.edu.cn (H. Yao), zhangzht@ccmu.edu.cn (Z. Zhang).
[1] Zhengyang Yang, Huanhuan Chen, Peizheng Yang and Xiaofei Shen contributed equally to this work.

https://doi.org/10.1016/j.biomaterials.2022.121401
Received 2 September 2021; Received in revised form 20 January 2022; Accepted 26 January 2022
Available online 28 January 2022

was proposed, which aims to partially administer hyperbaric dissolved oxygen into wet healing wounds, improving oxygen penetration and absorption in tissues [22,23]. However, to date, this method relies on hyperbaric oxygen generators, which are inconvenient to use and increase the risk of wound infection [24–26].

Considering that wound dressings are the most frequently used daily care products for patients with both moist healing and antibacterial functions, we believe that developing wound dressings to deliver moist oxygen will be a valuable improvement for chronic wound care. To achieve this goal, we report a lyophilized nanometre additive that can dissolve and deliver oxygen. This additive contains perfluorodecalin-encapsulated albumin nanoparticles (FDC@HSA), called nano-oxygenated (NOX) powder. As a safe oxygen-carrying material, perfluorodecalin is clinically used in vitreoretinal surgery and artificial blood and commonly studied to deliver oxygen in our previous works [27–29]. Consecutive nanoemulsifying and free-drying methods were further developed to make perfluorodecalin stable and easy to use in dressings.

Next, we mixed the NOX powder into a hyaluronate gel to form a nano-oxygenated gel (NOX-gel) and tested its synergistic ability with dressings through controlled experiments. The anti-hypoxia efficacy of NOX-gel was first confirmed by *in vitro* assays on hypoxic epithelial cells, endothelial cells and fibroblasts. Next, the oxygen delivery and healing ability were evaluated stepwise in a mouse acute wound model, diabetic chronic wound model and skin flap transplantation model. NOX was demonstrated to relieve cell hypoxia, accelerate healing and promote the survival of transplanted skin flaps. We believe that this invention has good prospects for transformation and application.

2. Results

Preparation and characterization. FDC@HSA was first prepared by ultrasound emulsification and high-pressure homogenization and then lyophilized into NOX powder under the action of protective agents. NOX-gel was further formed by mixing the lyophilized powder with clinical gel dressings such as hyaluronate and alginate. After application to wounds, NOX-gel was expected to deliver and release dissolved oxygen by perfluorodecalin nanoparticles to overcome local hypoxia and promote tissue regeneration (Fig. 1a).

In the following experiments, we chose the widely used 1% sodium hyaluronate gel as the matrix of NOX-gel and the experimental control group. Blank hyaluronate gel (Gel), hyaluronate gel containing only human serum albumin (Gel + albumin), NOX powder, and NOX-containing hyaluronate gel (NOX-gel) were separately photographed. NOX powder dissolved and dispersed well in hyaluronate gel, and NOX-gel appeared milky white because of the presence of perfluorodecalin nanodroplets (Fig. 1b). Nanoparticles were observed in NOX-gel under an electron microscope (Fig. 1c), and the average hydrodynamic diameter of the NOX-gel measured by dynamic light scattering was approximately 496.3 nm (Fig. 1d). Additionally, the oxygen

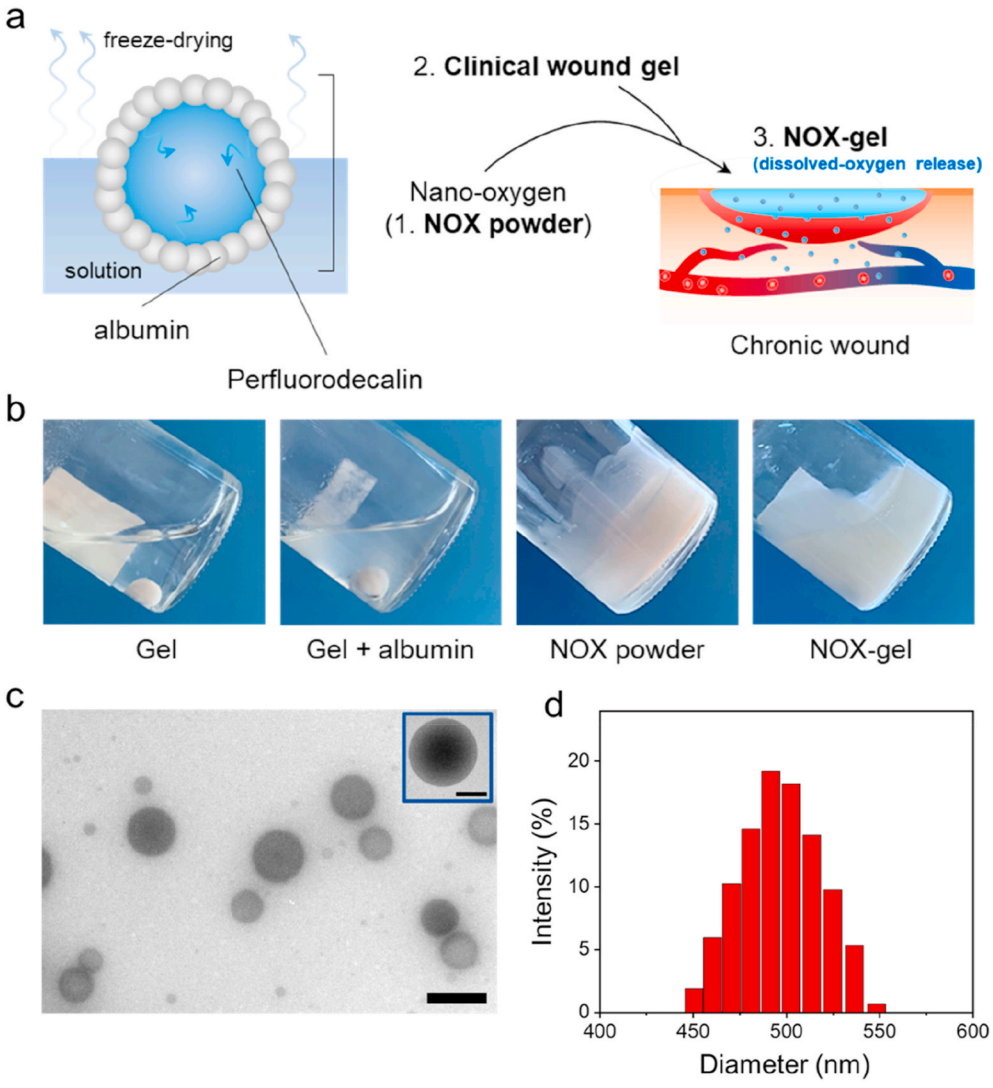

Fig. 1. Schematic diagrams and characterizations of NOX-gel. a Schematic illustration of the structure and chronic wound treatment of NOX-gel. 1. Structure and composition of NOX powder. 2–3. Once added into clinical wound gel and cover chronic wound, NOX-gel released the dissolved oxygen from itself to overcome local lower oxygenation. **b** Photographs of different kinds of gel. **c** TEM image of NOX-gel. The scale bars are 500 nm. Inset on the top right shows the high definition TEM results. The scale bars are 200 nm **d** Hydrodynamic diameter of NOX-gel.

concentration in NOX-gel was approximately 330 μmol/L, 360 μmol/L in FDC@HSA solution and 250 μmol/L in phosphate buffered saline (PBS), indicating little difference in the oxygen content before and after lyophilization (Fig. S1). These characterizations confirmed that FDC@HSA was successfully lyophilized and that the NOX-gel was well restored in use.

NOX-gel enhances cell migration and angiogenesis *in vitro*. Wound healing involves many cell types. Herein, we selected three key cell lines—keratinocytes, endothelial cells and fibroblasts—and the effects of NOX-gel on different cell lines were evaluated *in vitro*. To simulate the hypoxic injury environment, an extensively used hypoxia-mimetic agent, $CoCl_2$, was used and coincubated with cells to block degradation, further promoting the accumulation of hypoxia-inducible factor 1-α (HIF-1α) protein, which is a critical regulator of the cellular response to hypoxia [30–32]. The relative viability of human skin fibroblast (HSF) cells incubated with different concentrations of $CoCl_2$ was tested, and 600 μM $CoCl_2$ for 24 h was selected to mimic cellular hypoxia because of the half inhibitory concentration in cells (Fig. 2a).

The expression of HIF-1α in different groups was then monitored and quantified. Cells under normoxic conditions showed the lowest HIF-1α

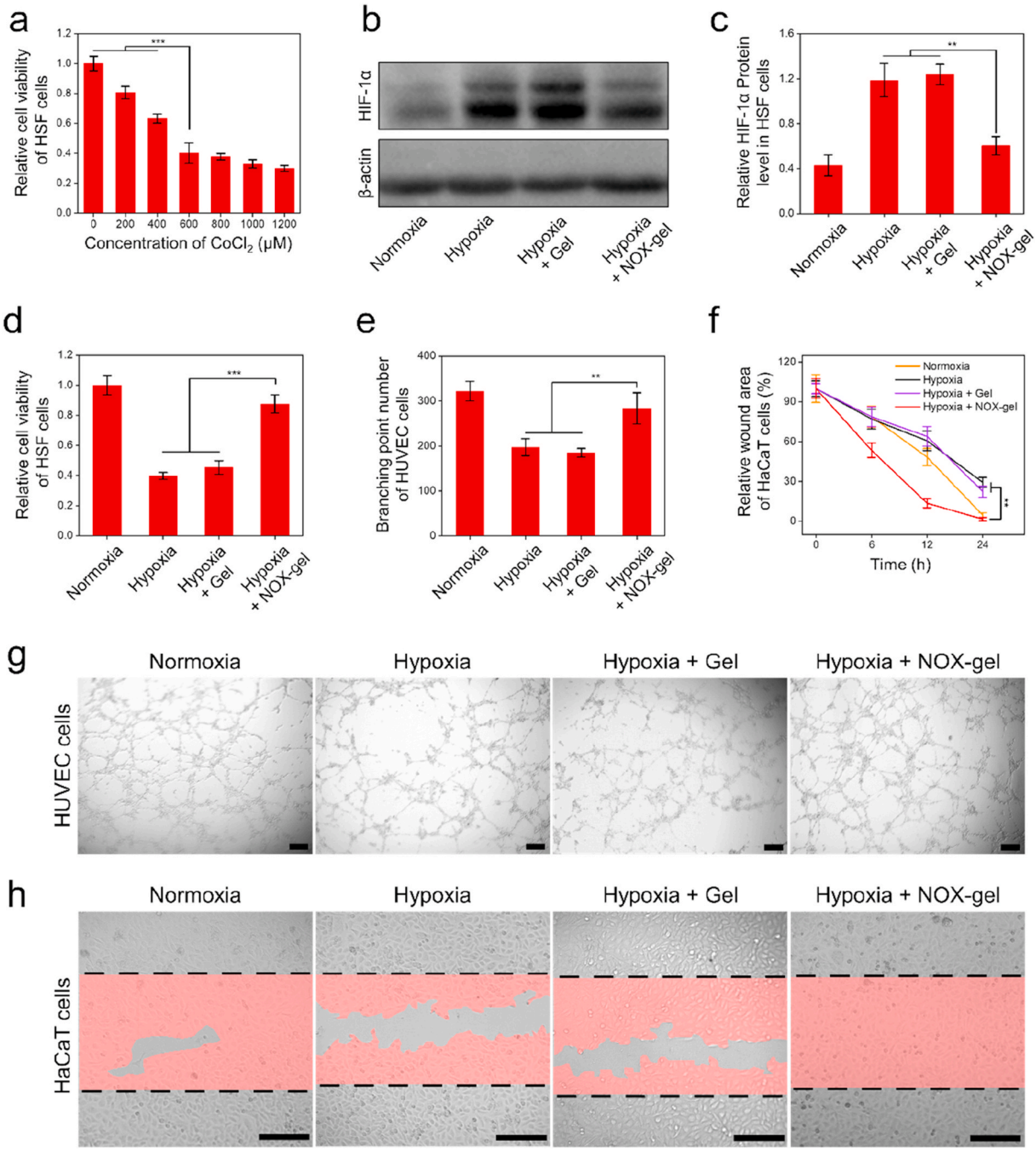

Fig. 2. *In vitro* cytotoxicity and therapeutic effect of wound healing using NOX-gel. a Relative cell viability of HSF cells after incubation with different concentration of $CoCl_2$ for 24 h. Data is shown as mean ± SD (n = 6). ***$p < 0.001$. **b, c** Western blots and quantitative analysis of HIF-1α protein level in HSF cell supernatant. Data is shown as mean ± SD (n = 3). **$p < 0.01$. **d** Relative cell viability of HSF cells using CCK-8 kit after various treatments. **e** Branching point number of HUVEC cells tube formation after various treatments. Data is shown as mean ± SD (n = 3). **$p < 0.01$. **f** Relative wound healing rate of HaCaT cells at different time points after various treatments. Data is shown as mean ± SD (n = 3). **$p < 0.01$. **g** The vasculogenic potential of HUVEC cells is determined by endothelial cell tube formation. The scale bars are 200 μm **h** The migration capability of HaCaT cells is determined by cell wound healing assay 24 h after wounded. The scale bars are 200 μm.

expression, hypoxic cells treated with or without Gel both showed the highest HIF-1α expression, and hypoxic cells treated with NOX-gel showed intermediate expression (Fig. 2b and c). These results confirmed that $CoCl_2$ (600 μM, 24 h) treatment successfully mimicked cellular hypoxia and led to high HIF-1α expression. Additionally, NOX-gel, but not normal gel, protected against hypoxia and downregulated HIF-1α. Fibroblast proliferation plays an essential role in wound healing. Next, we evaluated the relative cell viability, which indicated that the NOX-gel has notable granulation tissue potential by releasing oxygen, further reversing cell hypoxia for HSF proliferation (Fig. 2d). The relative HIF-1α and VEGF mRNA level in HSF cells performed similar trend in these four groups (Fig. S2a, b).

Angiogenesis is critical to recovering the continuous oxygen supply in chronic wounds. In this case, tube-formation experiments in human umbilical vein endothelial cells (HUVECs) were performed to identify the angiogenic capacity of NOX-gel. Fewer branching points were found

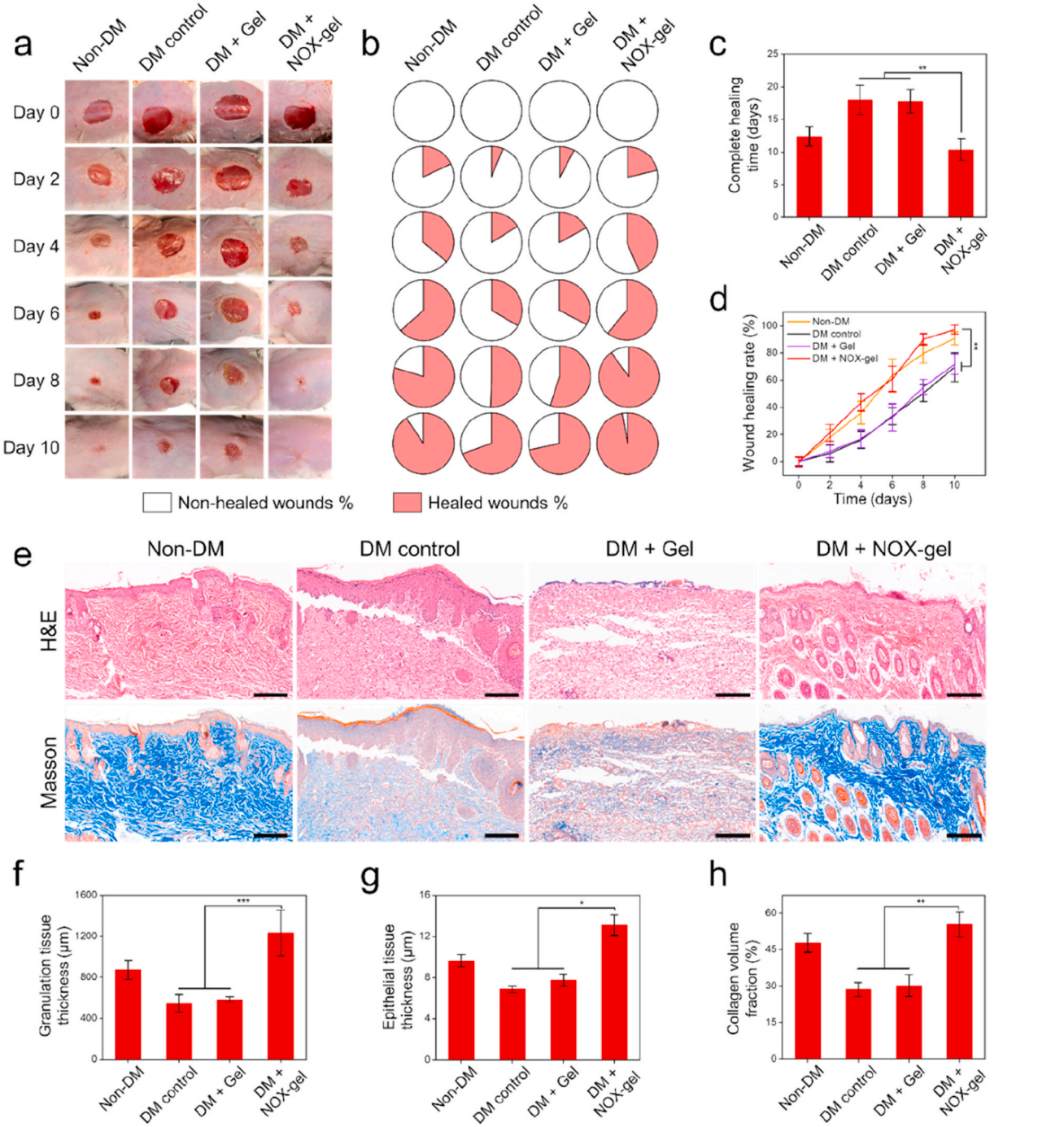

Fig. 3. NOX-gel promotes wound healing in diabetic mice. a Digital photograph of wounds healed at different time points after various treatments. **b** Healing fraction of wound in diabetic mice at different time points after various treatments. **c** Complete healing time in diabetic mice after various treatments. **d** Healing rate of wound in diabetic mice at different time points after various treatments. **e** H&E and Masson staining of skin tissue sections ten days after wounding. The scale bars are 100 μm **f** Granulation tissue thickness of skin tissues after various treatments through H&E staining. **g** Epithelial tissue thickness of skin tissues after various treatments through Masson staining. **h** Collagen volume fraction of skin tissues after various treatments through Masson staining. Data is shown as mean ± SD (n = 6). $^{*}p < 0.05$, $^{**}p < 0.01$ and $^{***}p < 0.001$.

in the hypoxia and hypoxia + Gel groups than in the normoxia group, illustrating that hypoxia inhibited cell vasculogenic potential (Fig. 2e, g). Interestingly, the branching point number was increased significantly in the hypoxia + NOX-gel group (**$p < 0.01$), indicating that enhanced vessel formation likely occurred because of oxygen delivery from the NOX-gel.

The migration of keratinocytes plays a critical role in re-epithelialization and wound closure, and the ability of NOX-gel to promote the migration of hypoxia-induced human immortalized keratinocytes (HaCaTs) was investigated using the scratch wound assay. Hypoxic cells treated with NOX-gel migrated and filled the scratch within 24 h, control hypoxic cells and hypoxic cells with hyaluronate gel treatment both failed to complete the migration within 24 h; the wound area was still present in the hypoxia (29.29% ± 3.77%) and hypoxia + gel (22.43% ± 4.18%) groups, respectively (Fig. 2f, h). Cells treated with NOX-gel for 24 h exhibited almost no wound area. The scratch wound assay images of each group at different time points (0, 6, 12, 24 h) are shown in Fig. S3. Additionally, wound healing assay of normal human epidermal keratinocytes (NHEK) exhibited the same trend (Fig. S4a, b). Thus, NOX-gel can support keratinocyte migration and proliferation in a hypoxic environment.

NOX-gel promotes acute and chronic diabetic wound healing. To verify whether NOX-gel can enhance cell proliferation and angiogenesis *in vivo*, we first evaluated NOX-gel in an acute wound healing model without diabetes. Superior efficacy of NOX-gel was demonstrated, and wounds in the NOX-gel group healed faster than those in the other three groups (Fig. S5a). The wound area in the NOX-gel group was also significantly smaller 6 and 8 days after treatment (Fig. S5b). Additionally, increased granulation tissue thickness, affluent neovascularization and more collagen volume were observed following H&E and Masson staining of skin tissue 10 days after treatment with NOX-gel (Fig. S5c).

Next, we monitored the therapeutic effect of NOX-gel in a diabetes mellitus (DM) wound healing model to simulate chronic wound healing. A diabetic mouse model was prepared by streptozotocin injection and high-fat diet feeding. The body weight curves (Fig. S6a) and blood glucose values (Fig. S6b) in each group at different time points after wounding indicated the successful establishment of this diabetic model. The mice were divided into the following 4 groups: normal mice, diabetic mice, diabetic mice treated with Gel + albumin and diabetic mice treated with NOX-Gel.

Daily treatment of wounds with NOX-gel accelerated wound healing compared with untreated diabetic wounds and treatment with gel (Fig. 3a). Additionally, wounds in the DM + NOX-gel group healed faster than untreated wounds without diabetes (Fig. 3b). Furthermore, wounds required approximately 10.4 days to heal completely in the DM + NOX-gel group but approximately 18.0 days in the DM group (Fig. 3c). Compared with the DM group, the diabetic model treated with NOX-gel exhibited a significantly accelerated wound healing rate 4 days after treatment (Fig. 3d). Such successful rapid wound closure might be attributed to NOX-gel, which can transport oxygen to wound tissues, further alleviating lower oxygenation.

Additionally, H&E and Masson staining procedures were conducted for histopathological analysis (Fig. 3e). Wounds in the DM + NOX-gel group closely resembled the normal epidermis of intact skin with a multilayered epithelium structure. Granulation tissue thickness in the DM + NOX-gel group (1233.33 ± 222.88 μm) was significantly higher than that in the DM group (546.67 ± 86.05 μm) and Gel group (584.02 ± 26.51 μm). Additionally, epithelial tissue thickness exhibited the same trend as granulation in the four groups (Fig. 3f and g). Furthermore, wounds treated with NOX-gel generated significantly more collagen (blue stained) than those treated with other dressings (Fig. 3h). The above results identified that NOX-gel promoted the granulation, reepithelialization and collagen generation of refractory nonhealing wounds in diabetes.

NOX-gel attenuates hypoxia and promotes angiogenesis in diabetic wounds. To test whether the rapid wound closure of NOX-gel might be attributed to its delivery of oxygen to wound tissues, further alleviating lower oxygenation, additional immunohistochemistry (IHC) analysis with HIF-1α antibodies (brown cells) was performed, further proving that treatment with NOX-gel could successfully prevent hypoxia (Fig. 4a). Additionally, the HIF-1α-positive cell density in the DM + NOX-gel group was significantly lower 6 and 12 days after intervention, confirming that this gel could continuously ameliorate hypoxic conditions in diabetic wounds (Fig. 4b).

The number of microvessels plays a key role in wound healing, likely explaining why NOX-gel promoted rapid facilitation of refractory nonhealing wounds. CD31 staining (red stars) was further performed to monitor the neovascularization ability after various treatments during the wound healing process (Fig. 4c). Many more CD31-positive microvessels were observed in the DM + NOX-gel group (30.41 ± 2.52) than in the DM group (15.23 ± 1.53) and gel group (16.37 ± 2.08) 12 days after intervention (Fig. 4d). Additionally, the relative HIF-1α and VEGF mRNA level also demonstrated that NOX-gel could effectively ameliorate hypoxia for promoting angiogenic factors expression in diabetic wounds (Fig. S7a, b).

In addition to angiogenesis, local inflammation also plays a critical role in the wound healing process. IHC staining of CD68 (red arrows) was performed to monitor local inflammation after various treatments during the wound healing process (Fig. 4e). The CD68-positive macrophage density in the DM and gel groups was significantly higher than that in the DM + NOX-gel group 6 and 12 days after intervention, indicating that NOX-gel could alleviate local inflammatory reactions continuously, even in the early and middle stages of the wound healing process (Fig. 4F). These results indicate that NOX-gel can reduce inflammation, promote neovascularization and ameliorate hypoxic conditions, further facilitating refractory nonhealing wounds faster in diabetes.

Skin flap survival model and treatment. Severe chronic wounds usually require skin flap transplantation, but hypoxia can lead to a failure to establish a blood supply of the flap in time, leading to necrosis. We hypothesized that NOX-gel promoted random skin flap regeneration in a skin flap survival model. We established this model in a previous study [33]. Briefly, a 2 cm × 1 cm rectangular skin flap was elevated and separated from the underneath soft tissue; its connection with any blood vessel was then cut thoroughly (Fig. S8a-d). Non-diabetic and diabetic mice without treatment served as the control group; diabetic mice were also treated with normal gel and NOX-gel.

Next, the skin flap was covered to its primary position, and the hydrogel was injected on the corresponding skin flap for treatment. Transparent dressing was finally used to bandage the wound for continuous treatment. The body weight curves (Fig. S9a) and blood glucose values (Fig. S9b) in each group at different time points after moulding indicated the successful establishment of this diabetic model. The blood flow on the skin flap was monitored using Doppler flowmetry to identify whether the blood supply of the skin flap could be influenced by different treatments.

NOX-gel enhances skin flap survival and angiogenesis in diabetes. The skin flap survival rates were evaluated by monitoring blood flow using Doppler flowmetry, and the blood flow intensities were displayed in an ascending sequence of blue, green and red (Fig. 5a). The blood supply of the skin flap disappeared only in the cut-off area (three sides of the rectangle) at 0 days after modelling. As the day progressed, the blood supply of the skin flap in the DM and gel groups decreased, while that in the DM + NOX-gel group gradually recovered. Doppler imaging revealed that a large part of the skin flap in the DM and gel groups exhibited faint yellow necrosis, while only a small part of the skin flap in the control group was necrotic. Interestingly, the skin flap in the NOX-gel group exhibited a healthy red colour and looked like normal skin with an adequate blood supply (Fig. S10). Additionally, the average necrosis rate in the DM + NOX-gel group (4.21% ± 2.39%) was significantly lower than that in the control (27.87% ± 4.15%), DM (76.43% ±

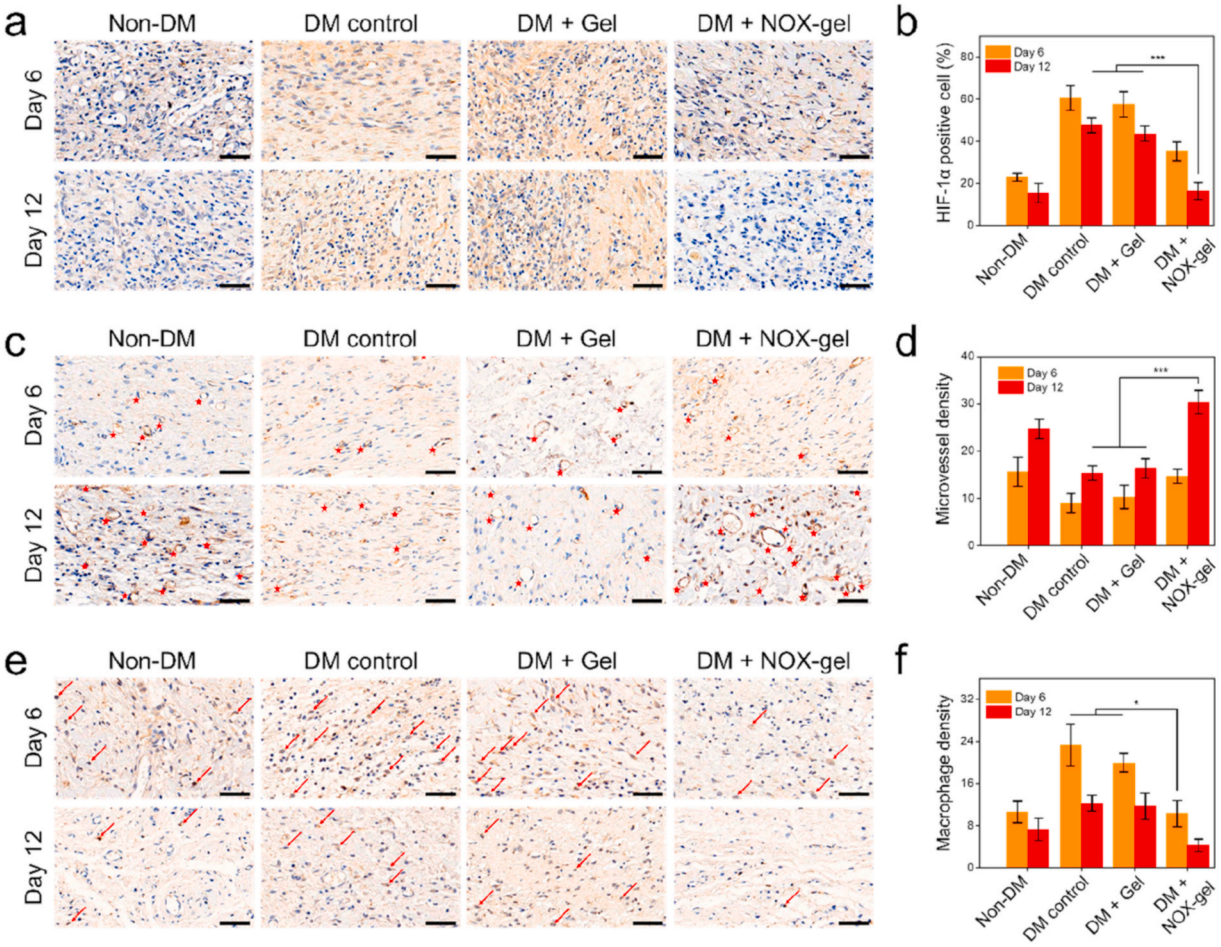

Fig. 4. Immunohistochemical results of skin tissue sections six and twelve days after wounding. a HIF-1α staining of skin tissue sections six and twelve days after wounding. The scale bars are 50 μm **b** The HIF-1α-positive cell density of each group six and twelve days after wounding. **c** CD31 staining of skin tissue sections six and twelve days after wounding. Red dots mark the endothelium cells and microvessels. The scale bars are 50 μm **d** The CD31-positive microvessels density of each group six and twelve days after wounding. **e** CD68 staining of skin tissue sections six and twelve days after wounding. Red arrows mark the CD68-positive macrophages. The scale bars are 50 μm **f** The CD68-positive macrophages density of each group six and twelve days after wounding. Data is shown as mean ± SD (n = 6). $^{*}p < 0.05$ and $^{***}p < 0.001$. (For interpretation of the references to colour in this figure legend, the reader is referred to the Web version of this article.)

7.54%) and gel groups (74.62% ± 4.62%) 6 days after treatment (Fig. 5b). The postoperative incision closure length in the DM + NOX-gel group grew the fastest, followed by that in the control group. The postoperative incision closure lengths in the DM and gel groups did not grow during the 6-day treatment (Fig. 5c).

H&E and Masson staining procedures were conducted for histopathological analysis (Fig. 5f and g). The granulation tissue thickness in the DM + NOX-gel group (647.23 ± 42.10 μm) was significantly higher than that in the DM group (422.69 ± 73.60 μm) and gel group (496.91 ± 11.79 μm) 6 days after treatment. Additionally, wounds treated with NOX-gel generated significantly more collagen (blue stained) than those treated with other dressings (Fig. 5e). The above results identified that NOX-gel promoted granulation and collagen generation, further increasing the skin flap survival rates in diabetes.

TdT-mediated dUTP nick-end labelling (TUNEL), Caspase-3, HIF-1α and vascular endothelial growth factor (VEGF) immunofluorescence (IF) staining of skin flaps was tested at Day 6. TUNEL and Caspase-3 staining was monitored to detect the apoptosis of transplanted skin flap tissue (Fig. 6a). The DM group had the most apoptotic skin cells, while NOX-gel effectively reversed apoptosis and promoted survival (Fig. 6b and c). The mechanism of VEGF in the healing of diabetic wounds has been comprehensively studied; in particular, VEGF promotes angiogenic actions by binding to the endothelial cell membrane [34]. To test our hypothesis that the delivered oxygen from NOX-gel promoted the survival of transplanted skin flaps, HIF-1α and VEGF staining was further performed to explore why NOX-gel increased the skin flap survival rates in diabetes. Consistent with the observations of hypoxia and angiogenesis in diabetic wound healing, HIF-1α expression in the DM + NOX-gel group was significantly lower 6 days after intervention, demonstrating that this gel could continuously transport oxygen to the diabetic skin flap, further ameliorating hypoxic conditions (Fig. 6d). The relative VEGF expression in the DM + NOX-gel group (151.61% ± 11.42%) was significantly higher than that in the DM group (39.98% ± 14.35%) and gel group (48.21% ± 10.54%), likely explaining why these dressings can protect the transplanted skin flap tissues from necrosis (Fig. 6d). These results indicated that NOX-gel could ameliorate hypoxic conditions, further promote the capability of neovascularization and protect skin flap tissues from necrosis, increasing the skin flap survival rates in diabetes.

3. Discussion

The healing of diabetic wounds is limited by an inadequate local oxygen supply. Considering that wound dressings are the most commonly used wound care for patients, we believe that dressings with an extra oxygen supply capacity can contribute to healing wounds, preventing gangrene and amputation, and they are more practical for patients than other oxygen delivery devices, such as chambers.

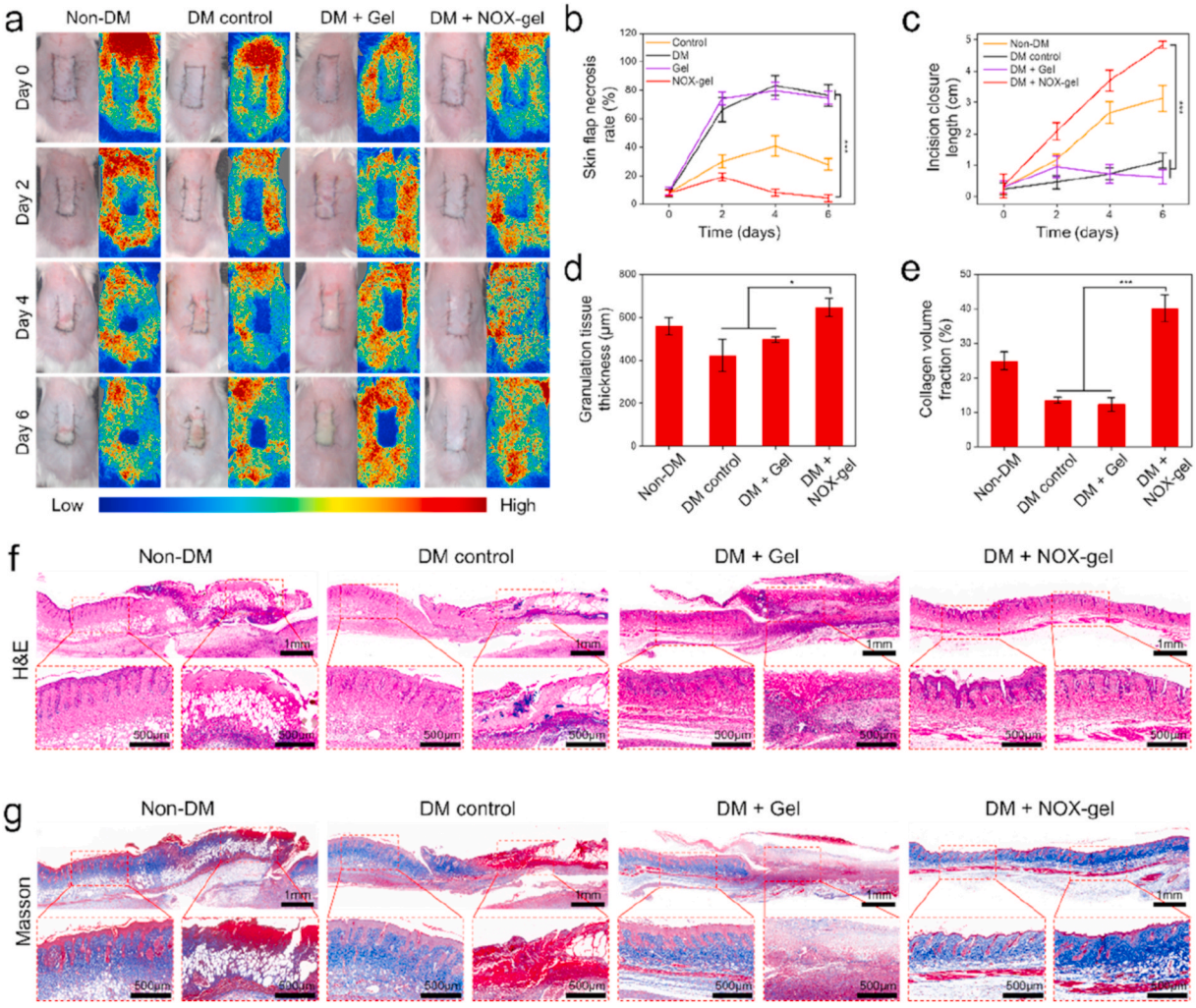

Fig. 5. NOX-gel promotes postoperative skin flap survival in diabetic mice. a Real-time blood flow images and digital photographs of skin flap survival at different time points after various treatments. **b** The postoperative necrosis rate of skin flap at different time points after various treatments. **c** The postoperative incision closure length at different time points after various treatments. **d** The granulation tissue thickness of each group six days after operation through H&E staining. **e** The collagen volume fraction of each group six days after operation through Masson staining. **f** H&E staining of the survival and necrosis junction area of skin flaps six days after operation. Panoramic photographs of H&E staining are at the top. The survival area is on the left lower part while necrosis area is on the right lower part. The scale bars are 1 mm and 500 μm, correspondingly. **g** Masson staining of the survival and necrosis junction area of skin flaps six days after operation. Panoramic photographs of Masson staining are at the top. The survival area is on the left lower part while necrosis area is on the right lower part. The scale bars are 1 mm and 500 μm, correspondingly. Data is shown as mean ± SD (n = 6). $^{*}p < 0.05$ and $^{***}p < 0.001$.

Based on our previous studies in perfluorocarbon-based oxygen delivery [27–29], we tried to add perfluorodecalin to gel dressings to prepare oxygenated wound gels. Importantly, perfluorodecalin liquid was clinically permitted as an eye surgery filler because of its biological inertness and in artificial blood because of its oxygen capacity [35,36]. Furthermore, we prepared nanoencapsulated perfluorodecalin for better wound penetration and lyophilized it into NOX powder for long-term stability. Currently, many oxygen-generating biomaterials have been reported and reviewed for tissue engineering for regenerative therapy, such as wound healing [37]. As Lyophilized products, NOX powder possess superior preservation and transport properties. Therefore, this invention can be universally mixed into each commercial gel dressing, showing good practical value for patient care.

Importantly, compared with normal hyaluronic gel, our hyaluronic gel with NOX (NOX-gel) promote cell migration capability, vasculogenic potential and cell viability by antagonizing the hypoxic environment in epithelial cells, endothelial cells and fibroblasts. Additionally, our data suggest a substantial curative effect on both chronic wound healing and skin flap survival diabetic mouse models using NOX-gel, which can reverse chronic wounds into acute healing and prolong the survival time of transplanted skin flaps. Considering the superior curative effect, we believe that it has good clinical transformation value to accelerate the healing of various wounds. Additionally, NOX-gel worked as moist oxygen delivered wound dressings at normal atmospheric pressure. Such approach could only relieve hypoxic conditions without achieving excessive oxygen content than normal tissues and causing hyperoxygenation damage to the tissue. The *in vitro* (Fig. S11a-c) and *in vivo* (Fig. S12a-c) results also demonstrated the considerations that ROS generation exhibited no significant difference between control and NOX-gel conditions.

In summary, the crude material of these NOX additive agents contains perfluorocarbons and human serum albumin, which have demonstrated excellent biosafety *in vivo*. Additionally, NOX also effectively overcame the risk of infection with superior preservation and transportation. Considering the above superior characteristics, our NOX technique can be used in diverse biomedical and clinical applications, such as the preservation of transplanted tissue and organs and is not limited to wound healing.

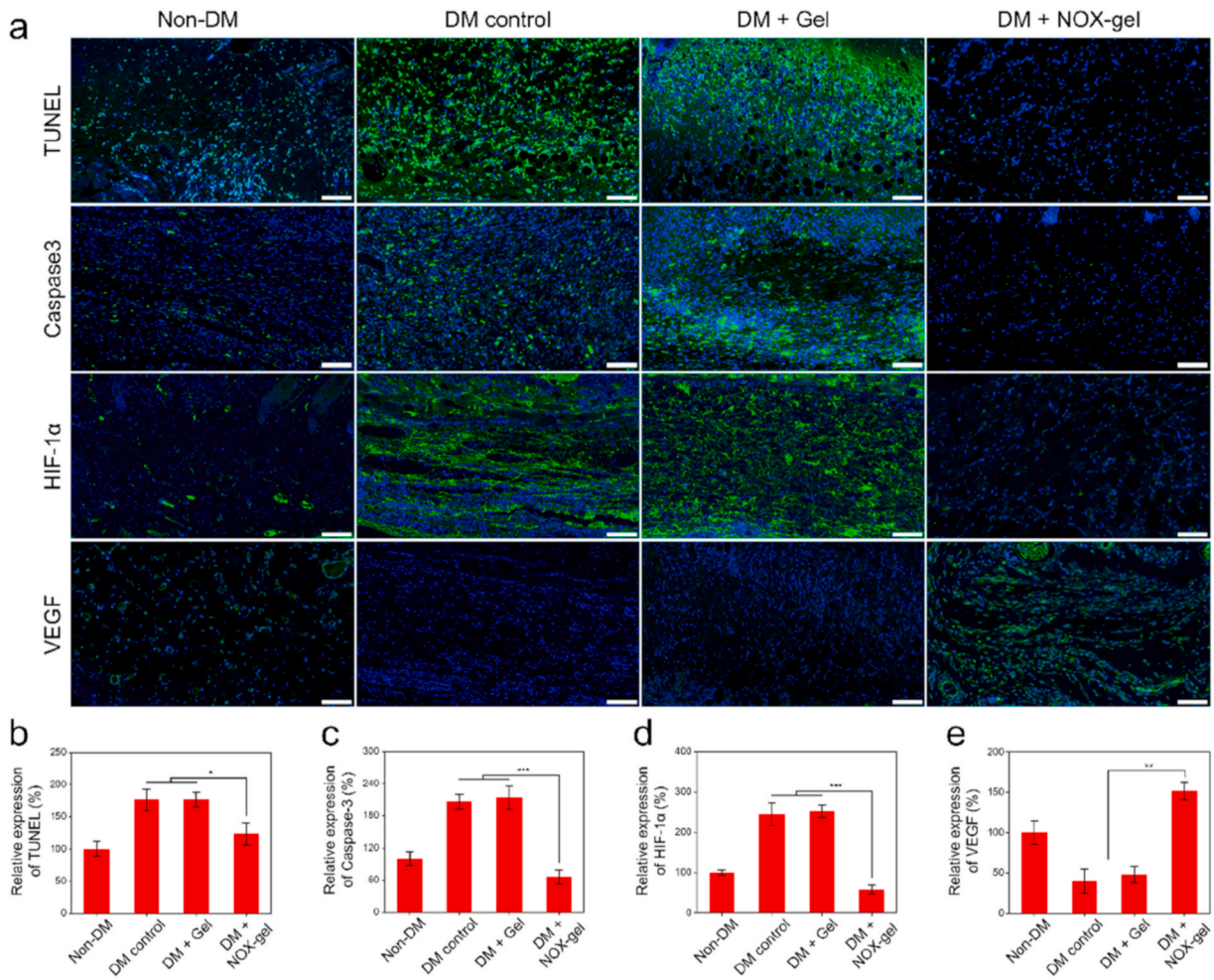

Fig. 6. Immunofluorescence results of skin flap sections six days after operation. a TUNEL, Caspase-3, HIF-1α and VEGF immunofluorescence staining of skin flap sections 6 days after operation. The scale bars are 100 μm **b** Relative TUNEL expression of each group six days after operation. **c** Relative Caspase-3 expression of each group six days after operation. **d** Relative HIF-1α expression of each group six days after operation. **e** Relative VEGF expression of each group six days after operation. Data is shown as mean ± SD (n = 6). $^{*}p < 0.05$, $^{**}p < 0.01$ and $^{***}p < 0.001$.

4. Methods

Preparation of Gel and NOX-gel. 10% hyaluronic acid and 4% human serum albumin (200 mg/mL) were added into phosphate buffer saline (PBS), and stirred for 24 h at ordinary temperature to get Gel. FDC@HSA were synthesized according to our previous studies [27–29]. In briefly, 2.5 mL human serum albumin and dithiothreitol were added into 10 mL deionized water to stir for 10 min, then, added 1 mL alcohol (ethanol, 99.5%) into the above solution and continued stirring for 3 min. Next, 1.5 mL perfluorodecalin was added into the solution gradually in ice bath at 300 W ultrasound for 6 min. FDC@HSA were acquired by centrifugating and resuspended with 10 mL PBS. Finally, 100 mg hyaluronic acid was added into such solution and stirred for 24 h at ordinary temperature. The 10 mL NOX-gel was successfully composed contained 50 mg/mL human serum albumin, 150 μL/mL perfluorodecalin and 10 mg/mL hyaluronic acid. The oxygen content in PBS, FDC@HSA solution (before freeze-drying) and NOX-gel (after redissolution) were monitored through dissolved oxygen electrode.

Characterization of NOX-gel. FDC@HSA were firstly lyophilized to acquire NOX powder and then redissolved by PBS. The morphology of NOX-gel was examined using transmission electron microscopy (TEM, TECNAI F20, FEI Company, USA). The hydrodynamic diameter of NOX-gel was measured using dynamic light scattering (DLS, 90 Plus, Brookhaven Instruments Corp., USA).

Cells culture. The HSF, HaCaT and HUVEC cells were purchased from the Shanghai Cell Biology Institute of Chinese Academy of Sciences. The NHEK cells were purchased from PromoCell, Heidelberg, Germany. Different cells were placed in corresponding medium as supplemented with 10% heat-inactivated fetal bovine serum, 100 U/mL penicillin and 100 μg/mL streptomycin in 5% CO_2 at 37 °C (HSF cells in DMEM medium, HUVEC and HaCaT cells in RPMI-1640 medium). The NHEK cells were cultured in Keratinocyte Growth Medium 2 (PromoCell).

Measurement of cell viability. Cell Counting Kit-8 (CCK-8) assay were purchased form Beyotime Biotechnology to evaluate the cell viability. HSF cells were seeded at a density of 1×10^4 cells/well into the lower chamber of 24-well transwell inserts with 8-μm pore-sizedfilters (Corning, NY, USA) for 24 h. Then, different concentrations of $CoCl_2$ (0, 200, 400, 600, 800, 1000 and 1200 μM) were added into the lower chamber and therapeutic gels were added into the lower chamber for 24 h co-incubation. Next, the cell viability of HSF was detected with CCK-8 kit by microplate reader. The appropriate concentration of $CoCl_2$ was selected for subsequent experiments.

Detection of hypoxia condition in HSF cells. The HSF cells were divided into four groups to treated with Gel or NOX-gel. Whole Cell Lysis Assay were purchased from Keygen Biotechnology to extract total proteins in HSF cells. The extracted proteins were isolated on a 10% polyacrylamide gel and transferred to nitrocellulose membranes using the wet transfer protocol. The glyceraldehyde-3-phosphate dehydrogenase (GAPDH) and HIF-1α monoclonal antibody obtained from Abcam

Technology were incubated with membranes overnight at 4 °C. The bound antibodies with anti-rabbit secondary antibodies obtained from Santa Cruz Biotechnology were measured and visualized using Pierce chemiluminescent substrate. Finally, the western blotting results were photographed using FLICapture and analyzed using ImageJ software. As for the quantitative real-time polymerase chain reaction (qRT-PCR) results *in vitro*, HSF cells were divided into four groups to treated with Gel or NOX-gel. After various treatments, RNA was extracted through TRIzol reagent and subjected to reverse transcription using RevertAid First Strand cDNA Synthesis Kit. The relative HIF-1α and VEGF mRNA level in HSF cells were then calculated using GAPDH the internal control gene.

Tube-formation experiment. Matrigel® basement membrane matrix was mixed with RPMI-1640 medium in 1:2 ratio. Then, 300 μL mixture was added in each well and solidified for 30 min at 37 °C. HUVEC cells were then seeded into the lower chamber of 24-well plates (4×10^4 cells/well). Then different therapeutic gels were added to the lower chamber for co-incubation. Subsequently, the scratched area was photographed using Leica microscope 6 h after co-incubation. The branching point number of endothelial cell tube formation was calculated using ImageJ software.

Measurement of cell-migration capability. HaCaT and NHEK cells were seeded in the lower chamber of 24-well plates (4×10^4 cells/well) for 24 h. Next, cell surface was scratched along a straight line using 200 μL pipetting barrel to establish wounds in each well and washed by medium to remove cell debris. Then different therapeutic gels were added to the lower chamber for 24 h co-incubation. Subsequently, the scratched area was photographed using Leica microscope at indicated time points (0, 6, 12 and 24 h after wound). The relative wound healing rate was calculated using ImageJ software.

Acute wound healing model and treatment. Balb/C male mice (about 25 g in weight) were purchased from Model Animal Research Center of Nanjing University. All animal experiments were approved by the Institutional Animal Care and Use Committee of Nanjing University and strictly abide by the Guidelines for Care and Use of Laboratory Animals of Nanjing University. Balb/C mice were first anaesthetized with sodium pentobarbital, then their back hair was shaved using an electric clipper and disinfect using 70% ethanol. A round full-thickness wound with a radius of 1.5 cm was created on mice using ophthalmic scissors. Mice in the control group were disinfected using 70% ethanol, dried and then treated using PBS. Mice in Gel, Gel + albumin and NOX-gel group were disinfected using 70% ethanol, dried and then treated using 500 μL corresponding gel. To make the gel to deliver oxygen more efficiently, 3 M™ Tegaderm™ transparent dressing was used to bandage the wound. The wound area and wound image were monitored and photographed every 2 days until the wounds were completely healed. After 10 days, mice were sacrificed and their wound tissues were collected, washed with PBS for further histopathological analysis.

Chronic wound healing model and treatment. The Balb/C mice were fasted for 6 h firstly and then intraperitoneally injected concentration of 10 mg/mL streptozotocin ith the indicated dose (100 mg/kg mice). The diabetes mouse model was successfully established when its fasting blood glucose value exceeded 16.7 mmol/L for 3 days. Then, the diabetic mice were first anaesthetized with sodium pentobarbital, then their back hair was shaved using an electric clipper and disinfect using 70% ethanol. A round full-thickness wound with a radius of 1.5 cm was created on mice using ophthalmic scissors. Normal mice without diabetes were included in the Non-DM group. Diabetic mice were included in the DM, DM + gel and DM + NOX-gel groups. In the Non-DM and DM groups, mice were disinfected using 70% ethanol, dried and then treated using PBS. While, in the DM + gel and DM + NOX-gel groups, mice were disinfected using 70% ethanol, dried and then treated using 500 μL corresponding gel and with 3 M™ Tegaderm™ transparent dressing on the wound. The body weight, blood glucose value, wound area and wound image were monitored and photographed every 2 days. After 10 days, mice were sacrificed and their wound tissues were collected, washed with PBS and added into 4% paraformaldehyde fix solution for further histopathological and IHC analysis.

Histopathological, IHC and qRT-PCR analysis. For the histopathological analysis, paraffin sections of 6 and 12 days after treatment were stained with hematoxylin and eosin staining kit (H&E, Keygen Biotechnology) and Masson staining kit (Keygen Biotechnology) according to the manufacturer description. The histopathological images were acquired using Leica microscope. The granulation tissue thickness, epithelial tissue thickness and collagen volume fraction of skin tissues were analyzed and calculated using ImageJ software. For the IHC analysis, the slices were incubated with the CD68, CD31 and HIF-1α monoclonal antibody (Abcam Technology) overnight at 4 °C. Then, horseradish peroxidase conjugated goat anti-rat secondary antibody was added according to the manufacturer's protocol for another 30 min cocultured at 37 °C. The IHC images of these sections were acquired using Leica microscope. The CD68-positive macrophages density, CD31-positive microvessels density and HIF-1α-positive cell density were analyzed and calculated using ImageJ software. The RNA of skin wound tissues was extracted using TRIzol reagent according to the manufacturer's instructions and subjected to reverse transcription using RevertAid First Strand cDNA Synthesis Kit. The relative HIF-1α and VEGF mRNA level of skin wound tissues were then calculated using β-actin the internal control gene.

Skin flap survival model and treatment. The diabetic mice were anaesthetized and a 2 cm × 1 cm rectangular area in the dorsal side of mice was marked. Then, the mice were incised three sides of rectangle to separate the skin flap from the underneath soft tissue clearly, and completely cut off the connection of such skin flap with any blood vessel. Subsequently, to cover the skin flap back to its primary position completely and suture the incision according to its original condition carefully. In the Non-DM and DM groups, mice were disinfected using 70% ethanol, dried and then treated using PBS. While, in the DM + gel and DM + NOX-gel groups, mice were disinfected using 70% ethanol, dried and then treated using 1 mL corresponding gel. The 3 M™ Tegaderm™ transparent dressing was also used to bandage the wound for continuously treatment. The blood flow and necrosis on the skin flaps were monitored using moorVMS-LDF1-HP doppler flowmetry (Moor instruments). Briefly, the average necrosis rate was calculated as the ratio of necrotic area (blue as barely blood flow intensity) to total area (2 cm × 1 cm rectangular area). The body weight, blood glucose value, flap image and postoperative incision closure length were monitored and photographed every 2 days. After 6 days, mice were sacrificed and their treated skin flap tissues were collected, washed with PBS, and added into 4% paraformaldehyde fix solution for further analysis.

Histopathological and IF analysis. For the histopathological analysis, paraffin sections were stained with H&E and Masson staining kit according to the manufacturer description. The histopathological images were acquired using Leica microscope. The granulation tissue thickness and collagen volume fraction of skin tissues were analyzed and calculated using ImageJ software. For the IF analysis, the skin flap tissue sections were embedded into optimal cutting temperature (OCT) compound further cryo-sectioned into frozen sections with 8-μm-thick in liquid nitrogen. The sections were washed using ice-cold acetone to remove the OCT wrapped around them, continued washing with PBS and the unspecific antigens were then blocked with 5% BSA blocking solution for 1 h. Next, they were incubated with the HIF-1α, VEGF, TUNEL and Caspase-3 monoclonal antibody (Abcam Technology) overnight at 4 °C. Then, the FITC-conjugated goat anti-rat secondary antibody (cwbiotech) was added according to the manufacturer's protocol. The IF images of these sections were acquired using Leica confocal laser scanning microscope (CLSM). The relative HIF-1α, VEGF, TUNEL and Caspase-3 expression of each group were analyzed and calculated using ImageJ software.

ROS concentration in cells and chronic wound tissue. We used DCFH-DA fluorescent probes to evaluate the ROS scavenging ability of NOX-gel for promoting wound healing *in vitro*. The control group was cultured with DMEM, while NOX-gel group was added NOX-gel into the

upper chamber of 24-well transwell at 37 °C. After 24 h at room temperature, all the above HSF cells incubated with DCFH-DA fluorescent probes in dark for 30 min, were imaged under a CLSM and quantified using ImageJ software. As for chronic wound tissue, the skin flap tissue sections were embedded into OCT compound further cryo-sectioned into frozen sections with 8-μm-thick in liquid nitrogen. The sections were washed using ice-cold acetone to remove the OCT wrapped around them, continued washing with PBS and the unspecific antigens were then blocked with 5% BSA blocking solution for 1 h. Then, the slices were incubated with the antibody DCFH-DA at 4 °C overnight, after washed with PBS for three times, DAPI was used to stain nuclei for 10 min. The sections were imaged with fluorescence microscope and quantified using ImageJ software. The ROS concentration was detected through enzyme linked immunosorbent assay (ELISA). Human ROS ELISA Kit and Mouse ROS ELISA Kit were purchased from Shanghai Enzyme-linked Biotechnology (Shanghai, China). Briefly, the supernatant fraction of HSF cells and chronic wound tissues were collected performed the immunoassays according to the manufacturer's instructions. All assays were duplicated for three times and each sample was retested six times for quality control.

Statistical analysis. All statistical analyses were performed using the GraphPad Prism (version 5.01) software. Data is shown as mean ± standard deviation (SD). Student's t-test was used between two groups and one-way ANOVA was used to analyze means more than two groups, which were followed by the Student–Newman–Keuls tests for multiple comparisons. The $*p < 0.05$, $**p < 0.01$ and $***p < 0.001$ were considered as statistically significant difference.

Credit author statement

Zhengyang Yang: Methodology, Formal analysis, Investigation, Resources, Data curation, Writing – original draft and Visualization.; **Huanhuan Chen**: Methodology, Formal analysis, Investigation, Resources, Data curation and Visualization.; **Peizheng Yang**: Formal analysis, Investigation, Resources and Data curation.; **Yiqiao Hu**: Conceptualization and Methodology.; **Yuhao Cheng**: Conceptualization, Methodology, Validation, Writing – review & editing and Project administration.; **Hongwei Yao**: Conceptualization, Writing – review & editing, Supervision and Project administration.; **Zhongtao Zhang**: Conceptualization, Writing – review & editing, Supervision, Project administration and Funding acquisition.

Data availability statement

All the other data supporting the findings of this study are available within the article and its supplementary information files and from the corresponding author upon reasonable request.

Declaration of competing interest

All authors declare that they have no conflict of interests.

Acknowledgments

This work was supported by grants from the National Key Technologies R&D Program (No. 2015BAI13B09), National Key Technologies R&D Program of China (No. 2017YFC0110904), Clinical Center for Colorectal Cancer, Capital Medical University (No. 1192070313).

Appendix A. Supplementary data

Supplementary data to this article can be found online at https://doi.org/10.1016/j.biomaterials.2022.121401.

References

[1] K. Ogurtsova, et al., IDF Diabetes Atlas: global estimates for the prevalence of diabetes for 2015 and 2040, Diabetes Res. Clin. Pract. 128 (2017) 40–50.
[2] S.D. Wiviott, et al., Dapagliflozin and cardiovascular outcomes in type 2 diabetes, N. Engl. J. Med. 380 (2019) 347–357.
[3] P.S. Briquez, J.A. Hubbell, M.M. Martino, Extracellular matrix-inspired growth factor delivery systems for skin wound healing, Adv. Wound Care 4 (2015) 479–489.
[4] GBD 2013 Mortality and Causes of Death Collaborators, Global, regional, and national age–sex specific all-cause and cause-specific mortality for 240 causes of death, 1990–2013: a systematic analysis for the Global Burden of Disease Study 2013, Lancet 385 (2015) 117–171.
[5] N. Masood, et al., Silver nanoparticle impregnated chitosan-PEG hydrogel enhances wound healing in diabetes induced rabbits, Int. J. Pharm. 559 (2019) 23–36.
[6] V. Falanga, Wound healing and its impairment in the diabetic foot, Lancet 366 (2005) 1736–1743.
[7] R. Nunan, K.G. Harding, P. Martin, Clinical challenges of chronic wounds: searching for an optimal animal model to recapitulate their complexity, Dis. Model Mech. 7 (2014) 1205–1213.
[8] V. Vijayakumar, S.K. Samal, S. Mohanty, S.K. Nayak, Recent advancements in biopolymer and metal nanoparticle-based materials in diabetic wound healing management, Int. J. Biol. Macromol. 122 (2019) 137–148.
[9] M.B. Dreifke, A.A. Jayasuriya, A.C. Jayasuriya, Current wound healing procedures and potential care, Mater. Sci. Eng. Mater. Biol. Appl. 48 (2015) 651–662.
[10] L.H. Hitchman, et al., Extracorporeal shockwave therapy for diabetic foot ulcers: a systematic review and meta-analysis, Ann. Vasc. Surg. 56 (2019) 330–339.
[11] C.J. Wang, J.H. Cheng, Y.R. Kuo, W. Schaden, R. Mittermayr, Extracorporeal shockwave therapy in diabetic foot ulcers, Int. J. Surg. 24 (2015) 207–209.
[12] W.P. Li, et al., CO2 delivery to accelerate incisional wound healing following single irradiation of near-infrared lamp on the coordinated colloids, ACS Nano 11 (2017) 5826–5835.
[13] C.M. Desmet, V. Preat, B. Gallez, Nanomedicines and gene therapy for the delivery of growth factors to improve perfusion and oxygenation in wound healing, Adv. Drug Deliv. Rev. 129 (2018) 262–284.
[14] P.G. Rodriguez, F.N. Felix, D.T. Woodley, E.K. Shim, The role of oxygen in wound healing: a review of the literature, Dermatol. Surg. 34 (2008) 1159–1169.
[15] A.A. Tandara, T.A. Mustoe, Oxygen in wound healing–more than a nutrient, World J. Surg. 28 (2004) 294–300.
[16] S. Schreml, et al., Oxygen in acute and chronic wound healing, Br. J. Dermatol. 163 (2010) 257–268.
[17] C.K. Sen, The general case for redox control of wound repair, Wound Repair Regen. 11 (2003) 431–438.
[18] H. Thangarajah, et al., HIF-1alpha dysfunction in diabetes, Cell Cycle 9 (2010) 75–79.
[19] Y. Zhu, Y. Wang, Y. Jia, J. Xu, Y. Chai, Roxadustat promotes angiogenesis through HIF-1alpha/VEGF/VEGFR2 signaling and accelerates cutaneous wound healing in diabetic rats, Wound Repair Regen. 27 (2019) 324–334.
[20] J. Golledge, T.P. Singh, Systematic review and meta-analysis of clinical trials examining the effect of hyperbaric oxygen therapy in people with diabetes-related lower limb ulcers, Diabet. Med. 36 (2019) 813–826.
[21] H. Kaldirim, S. Yazgan, B. Ceylan, K. Atalay, The effect of hyperbaric oxygen therapy on retinal thickness and progression of retinopathy in patients with Type 2 diabetes: a prospective cohort study, Cutan. Ocul. Toxicol. 38 (2019) 233–239.
[22] I.E. Gabbay, M. Gabbay, U. Gabbay, Diabetic foot cellular hypoxia may be due to capillary shunting–a novel hypothesis, Med. Hypotheses 82 (2014) 57–59.
[23] D.F. Roe, B.L. Gibbins, D.A. Ladizinsky, Topical dissolved oxygen penetrates skin: model and method, J. Surg. Res. 159 (2010) e29–36.
[24] P. Ceponis, C. Keilman, C. Guerry, J.J. Freiberger, Hyperbaric oxygen therapy and osteonecrosis, Oral Dis. 23 (2017) 141–151.
[25] G. Han, R. Ceilley, Chronic wound healing: a review of current management and treatments, Adv. Ther. 34 (2017) 599–610.
[26] D. Mathieu, A. Marroni, J. Kot, Tenth European Consensus Conference on Hyperbaric Medicine: recommendations for accepted and non-accepted clinical indications and practice of hyperbaric oxygen treatment, Diving Hybrid Med. 47 (2017) 24–32.
[27] P. Yu, et al., Artificial red blood cells constructed by replacing heme with perfluorodecalin for hypoxia-induced radioresistance, Adv. Ther. 2 (2019).
[28] Z. Zhou, et al., Two-stage oxygen delivery for enhanced radiotherapy by perfluorocarbon nanoparticles, Theranostics 8 (2018) 4898–4911.
[29] Z. Zhou, et al., Perfluorocarbon nanoparticles mediated platelet blocking disrupt vascular barriers to improve the efficacy of oxygen-sensitive antitumor drugs, Small 14 (2018), e1801694.
[30] H.R. Lee, F. Leslie, S.M. Azarin, A facile in vitro platform to study cancer cell dormancy under hypoxic microenvironments using CoCl2, J. Biol. Eng. 12 (2018) 12.
[31] M. Orozco-Ibarra, et al., Aged garlic extract and S-allylcysteine prevent apoptotic cell death in a chemical hypoxia model, Biol. Res. 49 (2016) 7.
[32] S.Y. Yoo, et al., Neuregulin-1 protects neuronal cells against damage due to CoCl2-induced hypoxia by suppressing hypoxia-inducible factor-1alpha and P53 in SH-SY5Y cells, Int. Neurourol. J. 23 (2019) S111–S118.
[33] H. Chen, et al., Dissolved oxygen from microalgae-gel patch promotes chronic wound healing in diabetes, Sci. Adv. 6 (2020) eaba4311.
[34] S.A. Almeida, et al., Murine strain differences in inflammatory angiogenesis of internal wound in diabetes, Biomed. Pharmacother. 86 (2017) 715–724.

[35] K.B. Ferenz, A.U. Steinbicker, Artificial oxygen carriers-past, present, and future-a review of the most innovative and clinically relevant concepts, J. Pharmacol. Exp. Therapeut. 369 (2019) 300–310.

[36] W. Liu, M. Gao, X. Liang, Management of subfoveal perfluorocarbon liquid: a review, Ophthalmologica 240 (2018) 1–7.

[37] N. Ashammakhi, et al., Advances in controlled oxygen generating biomaterials for tissue engineering and regenerative therapy, Biomacromolecules 21 (2020) 56–72.